



Antibacterial and catalytic activity of Cu doped ZnO nanoparticles: structural, optical, and morphological study

P. Raju^{1,4} · D. Deivatamil^{2,4} · John Abel Martin Mark³ · Joseph Prince Jesuraj³

Received: 6 March 2021 / Accepted: 18 July 2021 / Published online: 30 July 2021
© Iranian Chemical Society 2021

Abstract

Copper doped Zinc Oxide nanoparticles were synthesized using co-precipitation method. The structural optical, antibacterial activities were studied and compared with those of ZnO: Cu and the bare ZnO nanoparticles. XRD studies confirmed that all the prepared nanoparticles have hexagonal wurtzite structure of ZnO without any secondary phase after doping and the particle size was found to be within the range between 30 and 44 nm. By W–H (Williamson–Hall methods) analysis the strain occurred in ZnO and Cu: ZnO samples were calculated. UV–vis absorption spectra of the samples show sharp absorption edges around 290 nm. Optical absorption analysis of samples shows a red shift in the absorption band edge in Cu: ZnO nano-powders. The constituents of composites presence in Cu: ZnO samples were confirmed by FTIR data. The antibacterial activity of synthesized un-doped and Cu doped ZnO nano powders was studied using disc diffusion technique against both gram positive (*S. aureus*) and gram negative (*E. coli*) bacteria, which revealed the enhanced activity of Cu doped ZnO with increasing content of the doping agent. The catalytic activity of the prepared samples was analyzed with RhB (Rhodamine B) textile dye and 97% of efficiency was achieved for 5 wt% Cu doped ZnO nanoparticles within 6 min at pH 9.

Keywords Zinc oxide · Copper doped · Antibacterial activity · Catalytic property

Introduction

Owing to its wide band gap (3.37), and exciton-binding energy (60 meV), zinc oxide is a flexible and fascinating semiconductor material. ZnO has been applied to many fields such as light emitting diode, gas sensor, piezoelectric transducers, transparent conductive contacts, UV detectors, cosmetics, biomaterials, electronics, optics, photonics [1–10]. It has abundance in nature and eco-friendly property, inexpensive, toxic and chemically stable. Furthermore, its electrical and optical properties can be used in many

applications such as photoconductions, integrated sensors and transparent conduction oxides electrodes. S. Thota et al. has already discussed and reported the solubility of Ni, Co and Mn into the ZnO crystal lattices [11]. Cu is a fair substance as a doping material for ZnO among the various metallic dopants and the explanation is due to the increase in luminescence by producing localized impurity energy levels, have similar electronic shell structure, chemical identities and physical properties to those of Zn and the fact that it causes a shift in the optical properties and microstructure of the ZnO host compound [12]. Further copper has a capability to replace the atom of Zn easily because the ionic radii of Cu is close to the ionic radii of Zn [13, 14]. These characteristic make this material attractive for many applications such as solar cell, optical coating, photo catalysts, and electrical devices, UV photonic and transparent electronic applications [15–19]. Recently, micro- and nanostructured ZnO has been obtained by using various physical and chemical techniques. For the preparation of the Cu-doped ZnO nanostructure, numerous strategies were used, such as hydrothermal [20, 21], aqueous solution deposition [22], sol–gel processes [23, 24], mechano-chemical extraction [25, 26], spray pyrolysis [27, 28], and precipitation [29, 30], etc. Among all these

✉ Joseph Prince Jesuraj
josephprinceaut@gmail.com

¹ Post Graduate and Research Department of Physics, H. H. The Rajah's College, Pudukkottai, Tamilnadu 622001, India

² Department of Physics, Periyar E. V. R. College, Tiruchirappalli, Tamilnadu 620023, India

³ Department of Physics, University College of Engineering, Bharathidasan Institute of Technology Campus, Anna University, Tiruchirappalli, Tamilnadu 620024, India

⁴ Manonmaniam Sundaranar University, Abishekapatti, Tirunelveli, Tamilnadu 627012, India

routes, however, the precipitation approach, due to its simplicity and affordability, has gained more interest. Whereas the Cu-doped ZnO framework has been carried out by several scientists, a comprehensive study on the characteristics and especially the catalytic performance on organic dyes for Cu-doped ZnO nano-powders are still rarely reported according to our literature survey. Thus, the Cu-doped ZnO nanoparticles were synthesized by the process of co-precipitation and its catalytic cum anti-bacterial studies were analyzed and reported in the present work.

The comparative study of antibacterial active of pure and copper doped zinc oxide study is hardly available in literature survey to the best of our knowledge. Considering the above-mentioned points, in the present work, we have synthesized pure and Cu doped ZnO nanoparticles by co-precipitation and the antibacterial activity is studied by disc diffusion method.

Experimental

Materials

Analytical grade Merck brand with 99% purity, zinc acetate dihydrate ($\text{Zn}(\text{CH}_3\text{COO})_2 \cdot 2\text{H}_2\text{O}$), copper sulfate pentahydrate ($\text{CuSO}_4 \cdot 5\text{H}_2\text{O}$), sodium hydroxide pellets (NaOH), Sodium borohydride (NaBH_4), potassium bromide (KBr), Rhodamine B dye ($\text{C}_{28}\text{H}_{31}\text{ClN}_2\text{O}_3$) Sigma-Aldrich brand with 96% purity, and double distilled water (DD water) was used without any purification in experimental procedure.

Pure ZnO, Cu doped ZnO nanoparticles synthesis

Cu doped ZnO nanoparticles samples have been synthesized by precipitation method. For the pure ZnO nanoparticle synthesis, analytical grade zinc acetate dihydrate ($\text{Zn}(\text{CH}_3\text{COO})_2 \cdot 2\text{H}_2\text{O}$) having 0.5 M equivalent weight, was dissolved in 50 ml of de-ionized water to obtain a precursor solution. Using magnetic stirrer, homogeneous solution was obtained by stirring the solution continuously for half hour. Then, 2 g of NaOH was dissolved in 50 ml of de-ionized water and this solution was slowly added into zinc precursor solution with continuous stirring at normal room temperature up to getting white precipitate. The obtained precipitated was rinsed with de-ionized water several times and filtered. This product was dried in a vacuum air hot oven at 100 °C for 3 h and then calcined at 400 °C for 6 h for yielding pure ZnO nanopowder. Cu doped (1, 3, and 5 wt%) ZnO nanoparticles were prepared by dissolving copper sulfate ($\text{CuSO}_4 \cdot 5\text{H}_2\text{O}$) in the precursor ZnO solution and the remaining synthesis procedures were the same as that of the bare ZnO synthesis.

Characterization techniques

By using X ray diffraction (XRD) with analytical Model: X'Pert PRO, the crystal structure, lattice constants, strain and phase impurity were analyzed. Functional groups of samples were studied using Fourier transform infrared (FTIR) measurements with NICOLET AVATAR 360 Model. All spectra were recorded on pressed pellet of the prepared samples in potassium bromide (KBr). UV–Vis DRS were obtained using spectrophotometer Cary 5000. The surface morphology of the samples was examined using HITACHI S-3400.

Antibacterial activity

By disc diffusion method, the antibacterial activity of the ZnO and Cu doped ZnO nanoparticles was tested for *Escherichia coli* (Gram-negative) and *Staphylococcus aureus* (Gram-positive) bacteria by using Mueller–Hinton agar was used as a nutrient agar medium. The prepared medium was poured into petri plates and fresh bacterial cultures were spread over the plates by spread plate technique. The standard discs of 6 mm diameter containing nanoparticle samples (20 µg) were dispensed on to the petri plates. The plates were incubated at 37 °C for 24 h. After the incubation period, the diameter of the zone of inhibitions were measured and expressed in mm.

Catalytic studies of pure and Cu: ZnO nanoparticles

By observing the colour deterioration of the organic pollutant Rhodamine B dye, the catalytic performance of synthesized pure and Cu: ZnO nanostructures was determined. For this analysis, 10 mg/L dye solution was making up from that 10 ml of dye solution is mixed with 0.001 M of 10 ml NaBH_4 aqueous solution. 0.1 g of catalyst was dispersed thoroughly in 20 ml of double distilled water using ultrasonicate, and 5 ml of catalyst solution from the completely dispersed solution is taken and mixed with above-mentioned dye solution. The aliquots are collected regularly and investigated using UV spectrophotometer. The degradation percentage is acquired using the relation given below (Eq. 1) [31].

$$\eta = \left(1 - \frac{c}{c_0}\right) \times 100 (\%) \quad (1)$$

Result and discussion

XRD analysis

Figure 1 shows the X-ray diffraction of ZnO pure and Cu doped nanoparticles. The XRD patterns obtained were found to be composed of a ZnO hexagonal wurtzite structure with

wide peaks (JCPDS 36–1451) [16]. In XRD pattern, no additional impurity peaks were detected, indicating that; (1) Cu ions have been fully assimilated into the lattice of ZnO. This is due to the fact that ionic radius of Cu^{2+} (0.73 Å) [13] is very close to that of Zn^{2+} (0.74 Å) [14], due to which Cu can easily penetrate into ZnO crystal lattice 1, 3 and 5wt%. The crystallites size of unit cell parameters (a) and (c) of pure and Cu doped ZnO phases are represented in Table 1. The following relationship was used to acquire the lattice parameters of Cu: ZnO (Eq. 2) [32].

$$\frac{1}{d^2} = \frac{3}{4} \left(\frac{h^2 + k^2 + hk}{a^2} \right) + \frac{l^2}{c^2} \quad (2)$$

The lattice parameters of pure ZnO particles were $a = 3.2465$ Å, $c = 5.1992$ Å, which is similar to with a standard values [32]. For Cu–doped ZnO samples, the lattice parameters are slightly higher than pure ZnO. The diffraction peak for sample doped with 1, 3 and 5 wt% of Cu can be indexed to the hexagonal wurtzite structure of ZnO with

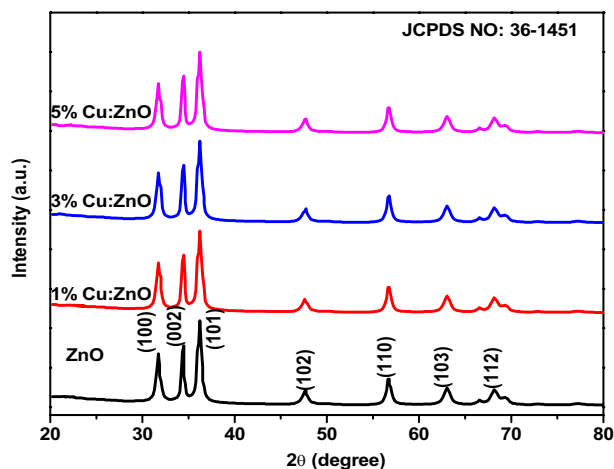


Fig. 1 XRD pattern of undoped ZnO—Nanoparticles and Cu doped ZnO—Nanoparticles

Table 1 Peak position 2θ , lattice constant (a & c), mean particle size (D) and micro-strain (ϵ) of Cu-doped ZnO nanoparticles

S. no.	Cu%	hkl (2θ)	d-spacing	Lattice parameters		D (nm)	ϵ (10^{-4})
				a (Å)	c (Å)		
1	Pure	(100) 31.8293	2.81154	3.2465	5.1992	31.1440	7.0865
		(002) 34.5024	2.59959				
2	1%	(100) 31.7945	2.81453	3.2504	5.2070	30.6460	7.7857
		(002) 34.4494	2.60347				
3	3%	(100) 31.7893	2.81498	3.2508	5.2061	24.7525	8.9999
		(002) 34.4554	2.60302				
4	5%	(100) 31.7772	2.81603	3.2517	5.2087	24.3811	9.3282
		(002) 34.4372	2.60436				

nine prominent peaks, clearly suggested that the samples are in single phase within detection limit. No detectable diffraction peak for any secondary or impurity phase such as CuO was found in both samples. Moreover, we can see the Bragg peaks at our Cu doped ZnO slightly move to lower angle side compared to that of the undoped samples. This indicates an important evidence of replacement of Zn^{2+} with Cu^{2+} ions.

The average crystallite size has been estimated by Debye–Scherrer equation (Eq. 3) [31].

$$D = \frac{0.9\lambda}{\beta \cos \theta} \quad (3)$$

where D is the average crystalline size, λ is the wavelength of the incident X-ray beam, θ is the Bragg's diffraction angle and β is the angular width of the diffraction peak at the half-maximum in radius on 2θ scale. The average crystallite sizes of the samples have been found to be 31 nm for pure and 31, 30, 24 nm and 24 nm for Cu doped sample.

Micro strain (ϵ) can be calculated using the formula (Eq. 4) [31]

$$\epsilon = \frac{\beta \tan \theta}{4} \quad (4)$$

It is observed that the strain in Cu doped samples varies with doping concentrations and is higher as the dopant is increased. The increased strain may be due to the incorporation of Cu ions in the regular sites of Zn ions in the ZnO lattice.

Fourier transforms infrared spectroscopy analysis

FTIR spectroscopy of Cu doped ZnO nanoparticles were taken in the range 4000 – 100 cm^{-1} and the results are shown in Fig. 2. A highly intense broad band has been observed at around 1470 cm^{-1} . A broad band has been observed at around 482 cm^{-1} for the pure ZnO is corresponding to the formation of Zn–O stretching vibration bond [30]. The FTIR spectra of the main absorption band are due to ZnO stretching of ZnO in the range of 500 – 482 cm^{-1} . The broad

band in the coupled Cu–ZnO at 699 cm^{-1} is assigned to the characteristic stretching mode of Cu–O bond, whereas other absorption bands found around [31], 1437 cm^{-1} are mainly due to C=C stretching [33]. The peaks in the range of 3781 cm^{-1} are due to the physical absorption of water H–O–H stretching and stretching and C–H stretching molecules by the carboxylic acid [33].

Optical properties

The room temperature UV–Vis DRS optical absorption spectrum of Cu:ZnO and wavelength ranges from 300 to 800 nm was recorded and illustrated in Fig. 3. The absorption edge varies from 320 to 390 nm for pure and Cu-doped ZnO nanoparticles. As 1 wt% of Cu is added into the Zn–O structure, the absorption edge is moved to its maximum shift, which may be due to the generated charge carriers.

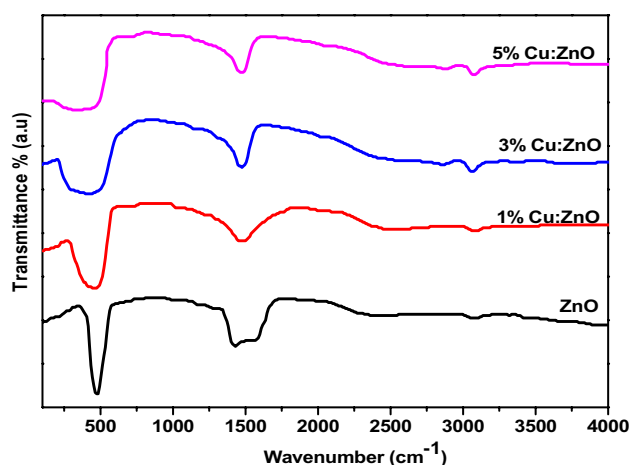


Fig. 2 FTIR spectrum of Cu doped ZnO nanoparticles

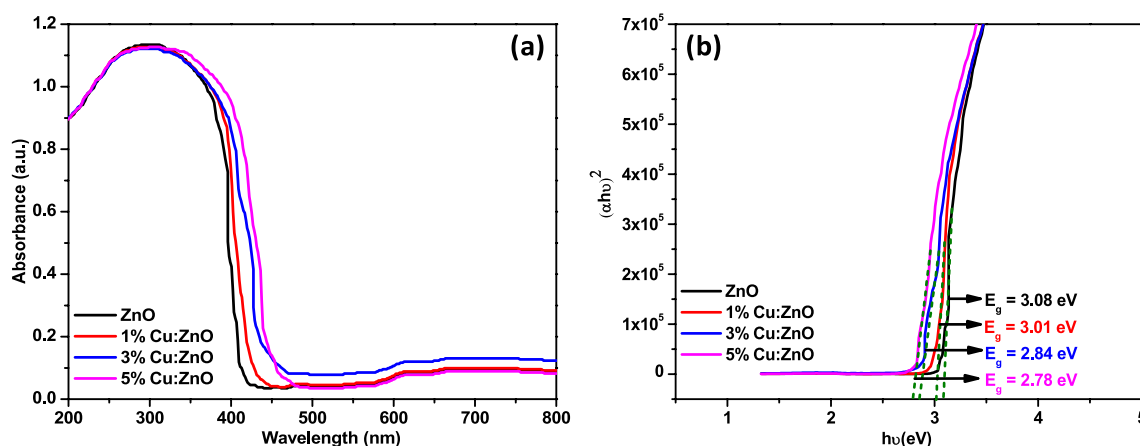


Fig. 3 a Optical absorption spectra of pure and Cu doped ZnO nanoparticles and b $(\alpha h\nu)^2$ versus bandgap energy of pure ZnO and Cu doped ZnO nanoparticles

Further increase in Cu dopant concentration beyond 5 wt%, the absorption is progressively red shifted because of the rise in lattice distortion as the Cu dopant concentration rose above 1 wt%. These distortion impacts the density of the carrier and the edges of absorption. With increasing Cu dopant, the position of the absorption spectra is blue-shifted. Using the Burstein-Moss effect, the widening of the band edge may explained [34]. The Fermi level shifts towards the conduction band, increasing the carrier concentration and increasing the energy difference in the band.

The optical band gap energy (E_g) of the semiconductor is calculated from Tauc's relation. A plot of $(\alpha h\nu)^2$ versus $h\nu$ shown intermediate linear region, the extrapolation of the linear part can be used to calculate the E_g from intersect with $h\nu$ axis as shown in Fig. 3b. For pure ZnO of wide band gap energy is 3.08 eV. For Cu doped ZnO (1, 3, and 5 wt %), the band gap energies are 3.01 eV, 2.84 eV, 2.78 eV, respectively, mentioned in Fig. 3b.

Surface morphological studies

SEM is a remarkably versatile technique that can be used to obtain information about the surface topography and composition. Figure 4a–d represents SEM micrographs of pure ZnO and Cu doped ZnO nanoparticles observed at $2\text{ }\mu\text{m}$ magnifications. The typical morphologies of Cu 1, 3, 5 wt% samples are found to be in cluster form of hierarchical structure, observed at $2\text{ }\mu\text{m}$ magnification. It is in good accordance with XRD results. All SEM results suggest that the shape and size of ZnO nanostructure prepared by precipitation method is highly depending on Cu additive. In addition the presence of O, Zn, and Cu in appropriate amounts and concentrations are determined by EDAX spectrum shown in Fig. 4a1, b1, c1 and d1, respectively, for ZnO and Cu 1, 3, 5 wt% doped ZnO nanoparticles.

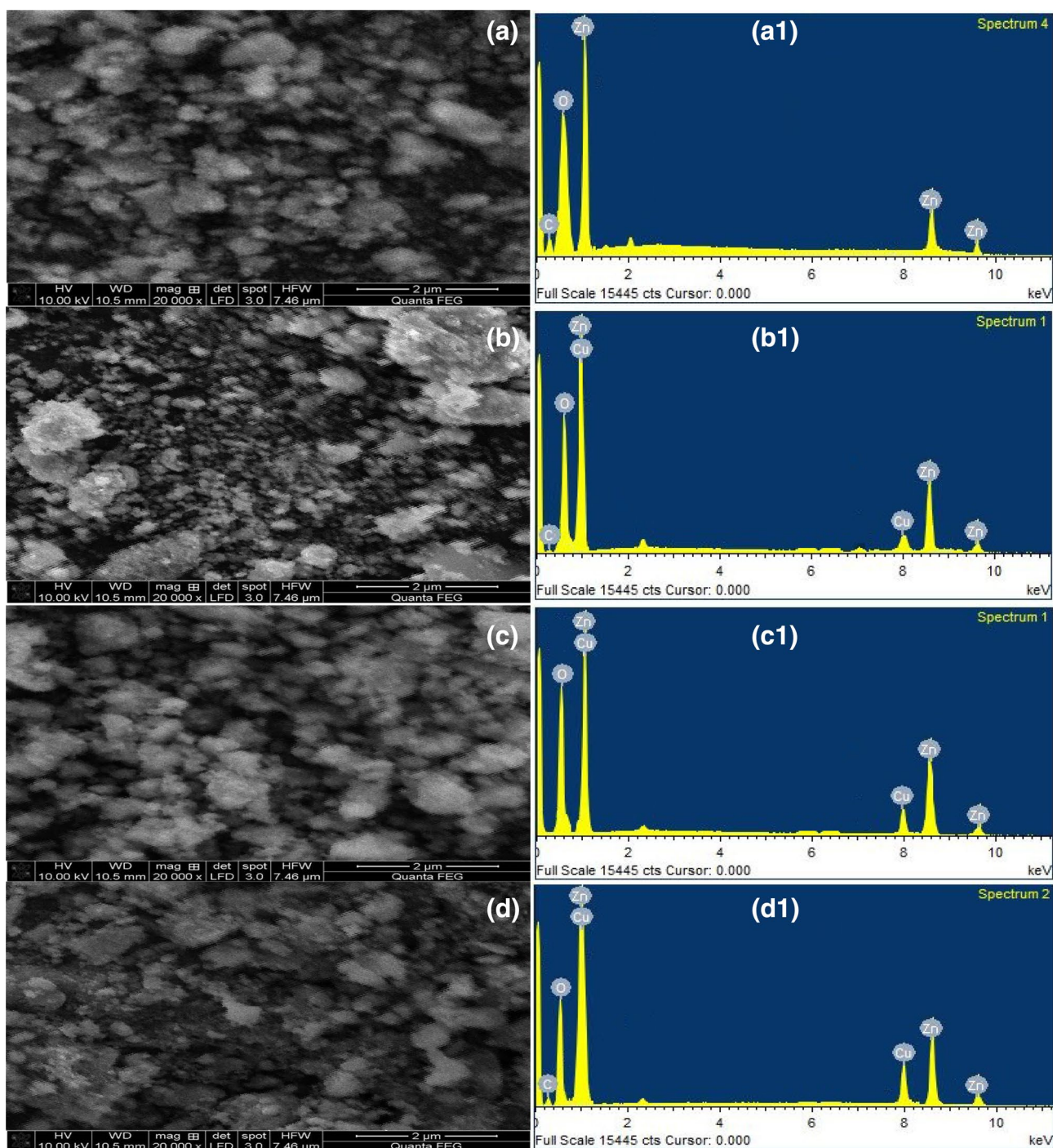


Fig. 4 SEM pictures of **a** ZnO, **b** 1% Cu: ZnO, **c** 3% Cu: ZnO, **d** 5% Cu: ZnO and nanoparticles observed at 2 μm magnifications and **a1** ZnO, **b1** 1% Cu: ZnO, **c1** 3% Cu: ZnO, **d1** 5% Cu: ZnO are the EDAX spectrum, respectively

Antibacterial application

The antibacterial activity of synthesized un-doped and Cu doped ZnO nano-powders was studied using disc diffusion technique against both gram positive (*S. aureus*) and gram negative (*E. coli*) bacteria. The zone of inhibition around

the disc is shown in Fig. 5a, b and the measured values of inhibition are given in Table 2. From Fig. 5a, b, it is noted that ZnO nano-powders show significant impact on the growth of bacteria around the disc. No inhibition zone was observed for control, prepared by the stock solution taken in disc without ZnO nano-powders. It can be observed that

the antibacterial activity of Cu doped ZnO nano-powders against all the bacteria remarkably increases compared to the un-doped ZnO nano-powders, this may be due the decrease in grain size as increasing Cu concentration in ZnO. The antibacterial activity of ZnO nano-powders should be associated with several mechanisms including (1) generation of Reactive Oxygen Species (ROS) like super oxide anions (O_2^-) and hydroxyl radicals ($OH\bullet$), (2) release of Zn^{2+} ions from the ZnO nano-powders which simply penetrate into the cell wall and they can cause severe damage to the bacteria and kill the bacteria and (3) small grain size. Moreover, nano-sized ZnO were attached to the bacteria and it disturbs the usual function of bacteria and hence they can damage severely to outer surface of the bacteria such as DNA, lipids and proteins. From Fig. 5a and b, it is found that 5 wt % of Cu doped ZnO nano-powders has robust antibacterial activity on *E. coli* and (Gram negative) than *S. aureus* (Gram positive) bacteria. This greater antibacterial activity against gram negative bacteria is ascribed to the variation in cell wall membrane of these bacteria. This greater antibacterial activity against gram negative bacteria is ascribed to the variation in cell wall membrane of these bacteria. The gram negative bacteria such as *E. coli* consist of its thickness range from (16, 20, 21, 23 nm) undoped and Cu doped at pure, 1, 3, 5 wt%, respectively. On the other hand, the gram positive *S. aureus* bacteria have a very thick cell wall membrane, its thickness range from (14, 18, 20, 22 nm) and made up of large number of mucopeptides, lipoteichoic and acids murein. In addition, *S. aureus* has an antioxidant enzyme and shows a strong oxidant resistance. Thus, super oxide anions, hydroxyl radicals and released Zn^{2+} ions can easily penetrate into *E. coli* and *S. aureus* and destroyed the bacteria. From

this it is concluded that the better inhibition is obtained for 5 wt% Cu doped ZnO nano-powders against all the bacteria.

Catalytic activity

The catalytic mechanism of deteriorating RhB dye is studied by monitoring UV–Vis spectrum each 60 s for 10 min, using $NaBH_4$ as a reducing agent and pure ZnO and Cu doped ZnO NPs as a catalyst. Relative to other agents, $NaBH_4$ is an effective reduction product and is also low toxic than other existing reducing agents. Even so, some sort of catalyst is required to carry out this reaction to make it faster. By reducing the activation energy, the catalyst (such as Cu: ZnO NPs) lowers the kinetic barrier between the donor BH_4^- and the acceptor RhB^+ . Catalytic reduction occurs when the donor BH_4^- and acceptor RhB^+ are adsorbed on the surface of ZnO NPs, and the electron is transferred from BH_4^- to RhB^+ , leading in the faster breakdown of RhB dye molecules. While the dye reduction shows fast progresses when adding the synthesized catalyst, pure ZnO and Cu doped ZnO NPs into the solution mixture of $NaBH_4$ and RhB dye, confirmed by the UV–Visible spectra shows the exponential reduction of the maximal peak intensity at 554 nm, and also rapid transition dye solution from colored to colourless over 10 min is displayed in Fig. 6a–e. Consequently, with regards to the ZnO and Cu: ZnO catalyst, the BH_4^- can behave as an electron donor (nucleophile) while the MB works as an electrophile. Therefore, the electrophile MB can obtain electrons from the catalyst and the nucleophile BH_4^- can supply the ZnO and Cu: ZnO catalyst with electrons. And thereby, for the RhB degradation in a $NaBH_4$ environment, the Cu: ZnO catalyst serves as such an electron conduit.

Fig. 5 **a** Antibacterial Activity of *Staphylococcus aureus* and **b** *Escherichia coli* for **c** control, (p) pure ZnO, (1%) 1% Cu: ZnO, (3%) 3% Cu: ZnO, (5%) 5% Cu: ZnO, respectively

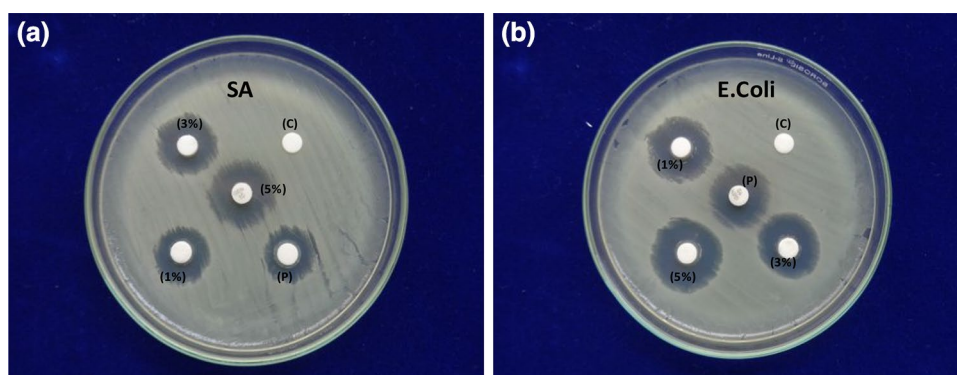


Table 2 Assay of antibacterial activity

S. no.	Bacteria	Zone of inhibition (mm in diameter)				
		Control	ZnO	1%Cu: ZnO	3%Cu: ZnO	5%Cu: ZnO
1	<i>Escherichia coli</i>	–	16	20	21	23
2	<i>Staphylococcus aureus</i>	–	14	18	20	22

Therefore, the catalyst produced by this approach can also be applied to different commercial processes. The energy of bond decomposition takes place at the moment of the chemical process, wherein the older bond is broken and new one built up. Hence, it leads to the complete

degradation of the dye molecules. In the reaction mixture, between RhB dye and BH_4^- ions, the prepared ZnO and Cu: ZnO catalyst acts as a prospective pathway for electron transfer. Therefore, in the presence of ZnO and Cu: ZnO catalyst the rate of the degradation reaction has raised.

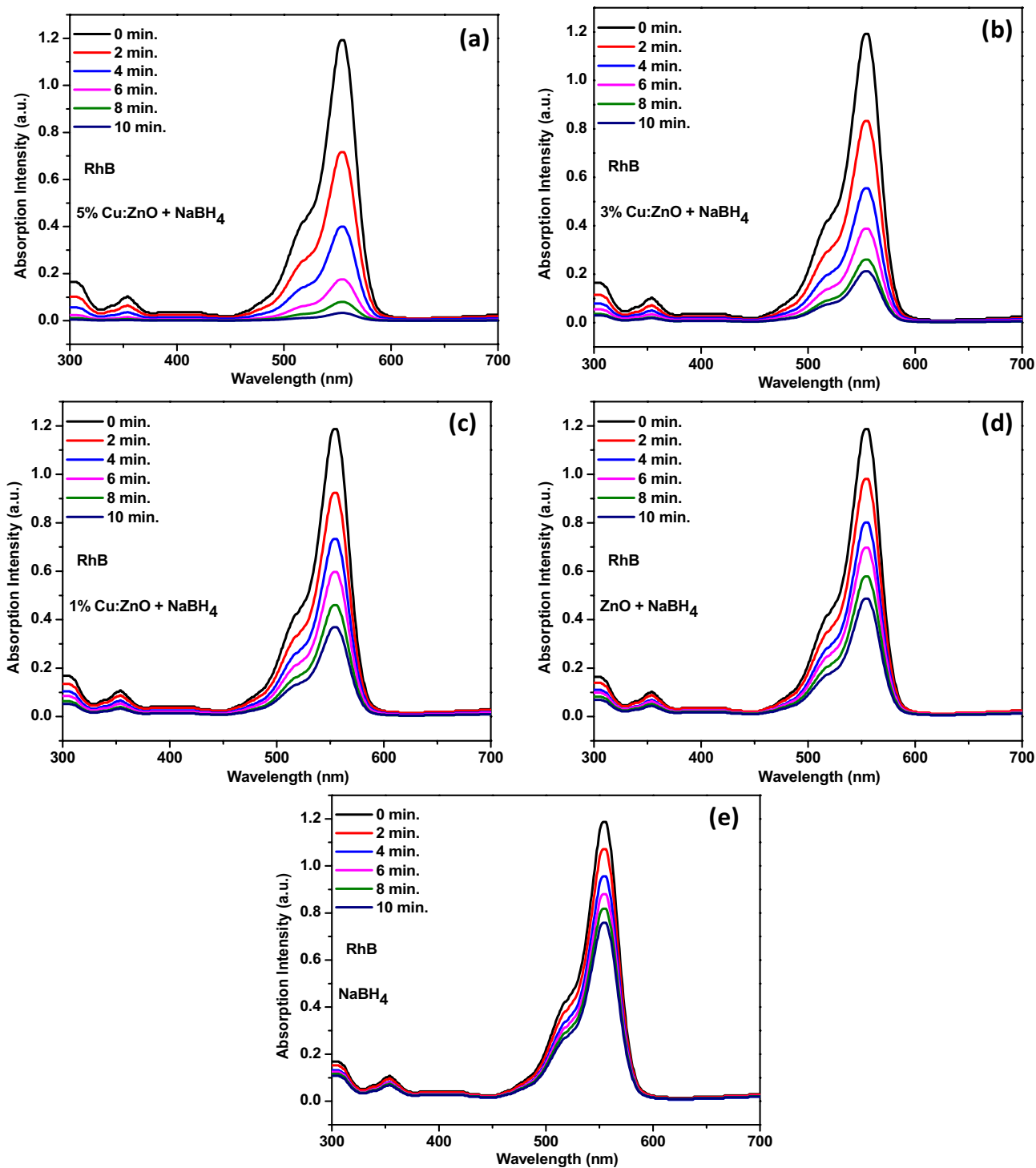


Fig. 6 a–e Time-dependent UV-absorption spectrum of RhB dye with respective catalysts

The C/C_0 regarding to the reaction time (t) for the decomposition of RhB by pure ZnO and Cu: ZnO catalyst is seen in Fig. 7a comparatively. Degradation efficiency (η) can be determined using Eq. 1. (Refer “Catalytic studies of pure and Cu: ZnO nanoparticles” section). The efficiency obtained is mapped with time duration and is seen in the figures. Also the inclusion of doping increases degradation efficiency which is proven from that figure. In the case of RhB dye catalytic degradation, the efficiency of degradation is high for 5 wt% doped ZnO NPs relative to all other synthesized products. Pseudo-first-order kinetics for the reduction of RhB dye can be used to measure the rate constant. The formula of reaction kinetics is shown below (Eq. 4) [31],

$$\ln\left(\frac{C}{C_0}\right) = kt \quad (4)$$

where (k) referred as the rate constant. The initial and final RhB concentrations are C_0 and C , accordingly. The difference of $\ln(C/C_0)$ towards reaction time for the destruction of RhB by ZnO and Cu: ZnO catalyst is illustrated in Fig. 7b.

Determination of point of zero charge (PZC) for the materials

Figure 8a depicts the PZC of the developed catalysts. The surface of the catalyst is negatively charged over the PZC, resulting in a strong columbic charge contact between the catalyst surface and the cationic RhB dye particles. Because of the electrostatic attraction above PZC, so much dye molecules are adsorbed on the catalyst's surface tends to result in a greater degrading performance, while the columbic electrostatic repulsion between the catalyst and the dye molecules results in a low effectiveness at acidic pH. We

discovered that the effectiveness is optimum near this highest surface charge point after conducting trials at various pH levels. This result holds true for both doped and undoped ZnO nanoparticles, indicating that at this pH 9, the largest negative charge causes the most adsorption.

Influence of pH in the degradation:

In catalytic breakdown reactions of dye molecules, the pH of the reaction mixture is essential. By introducing suitable doses of NaOH and HCl solutions to the experimental solution the acidic and alkaline pH of the solution was determined. Hence, the catalytic behaviour of better sample (5 wt% Cu: ZnO) was further analyzed by maintain the solution with different pH (3, 5, 7, 9, 11). Once the pH of the RhB dye solution is raised from 3, the catalytic degrading performance of prepared catalyst (5 wt% Cu: ZnO) progressively improves as seen in Fig. 8b. When compared to acidic and neutral pH, 4 and 7, the rate of dye molecule breakdown in the pH range 8–11 is significantly higher. It is noteworthy that for each of the four synthesized samples, Fig. 8b clearly shows the ideal pH required to achieve the best efficiency is 9. Figure 9a reveals the UV absorption spectrum of RhB dye with catalyst (5 wt% Cu: ZnO) at pH 9. We observed a drastic change in the catalytic behaviour for the 5 wt% Cu: ZnO sample at pH 9 that is it degrades up to 99% of RhB concentration within 6 min. This may due to the attraction of dye molecules on the surface of the catalyst material is much more in pH 9, so the catalyst may easily transfer the free electrons from NaBH_4 to dye molecule. The comparative C/C_0 versus time graph for bare NaBH_4 , NaBH_4 & 5 wt% Cu: ZnO and NaBH_4 & 5 wt% Cu: ZnO at pH 9 is seen in Fig. 9b and corresponding leaner fit graph is shown in Fig. 9c. The calculated rate constant, R^2 value, degradation

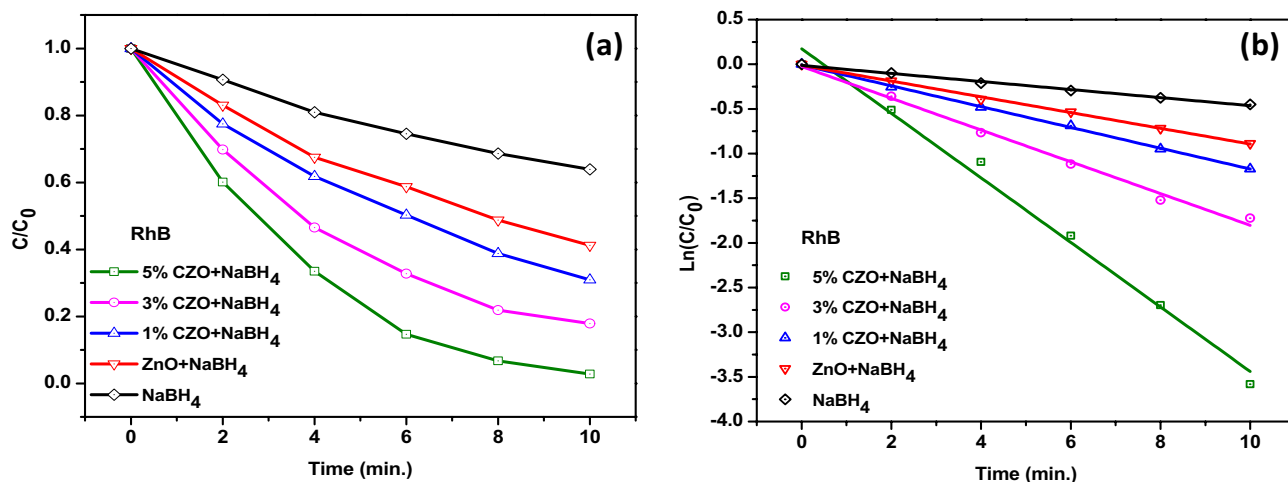


Fig. 7 a and b C/C_0 versus reaction time and $\ln(C/C_0)$ versus reaction time of RhB dye with respective catalysts

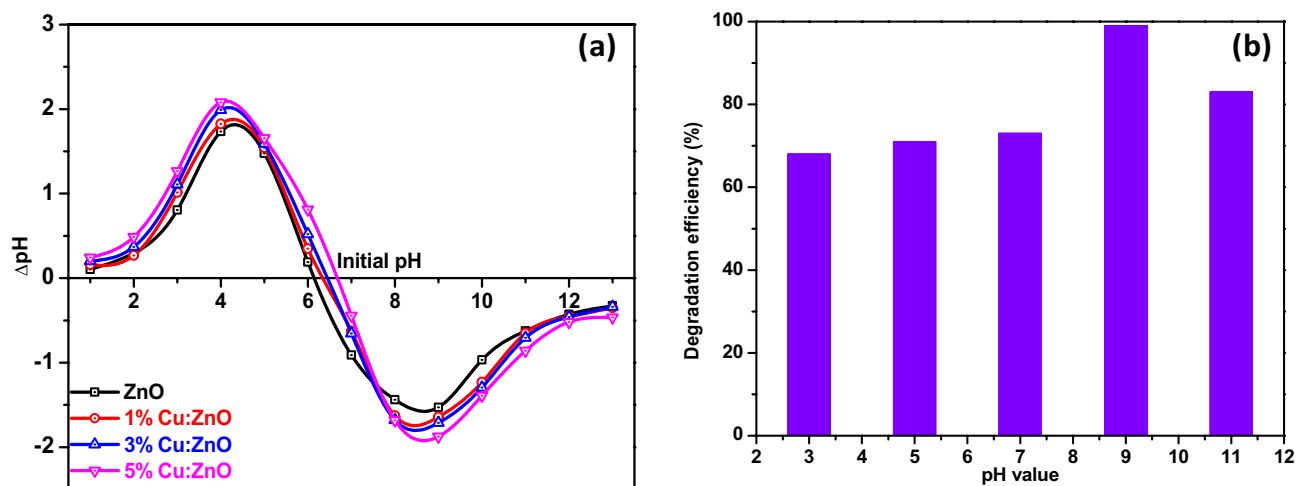


Fig. 8 **a** PZC measurements for ZnO and Cu doped ZnO nanoparticles. **b** Degradation percentage of RhB dye with catalyst (5 wt% Cu: ZnO) at different pH

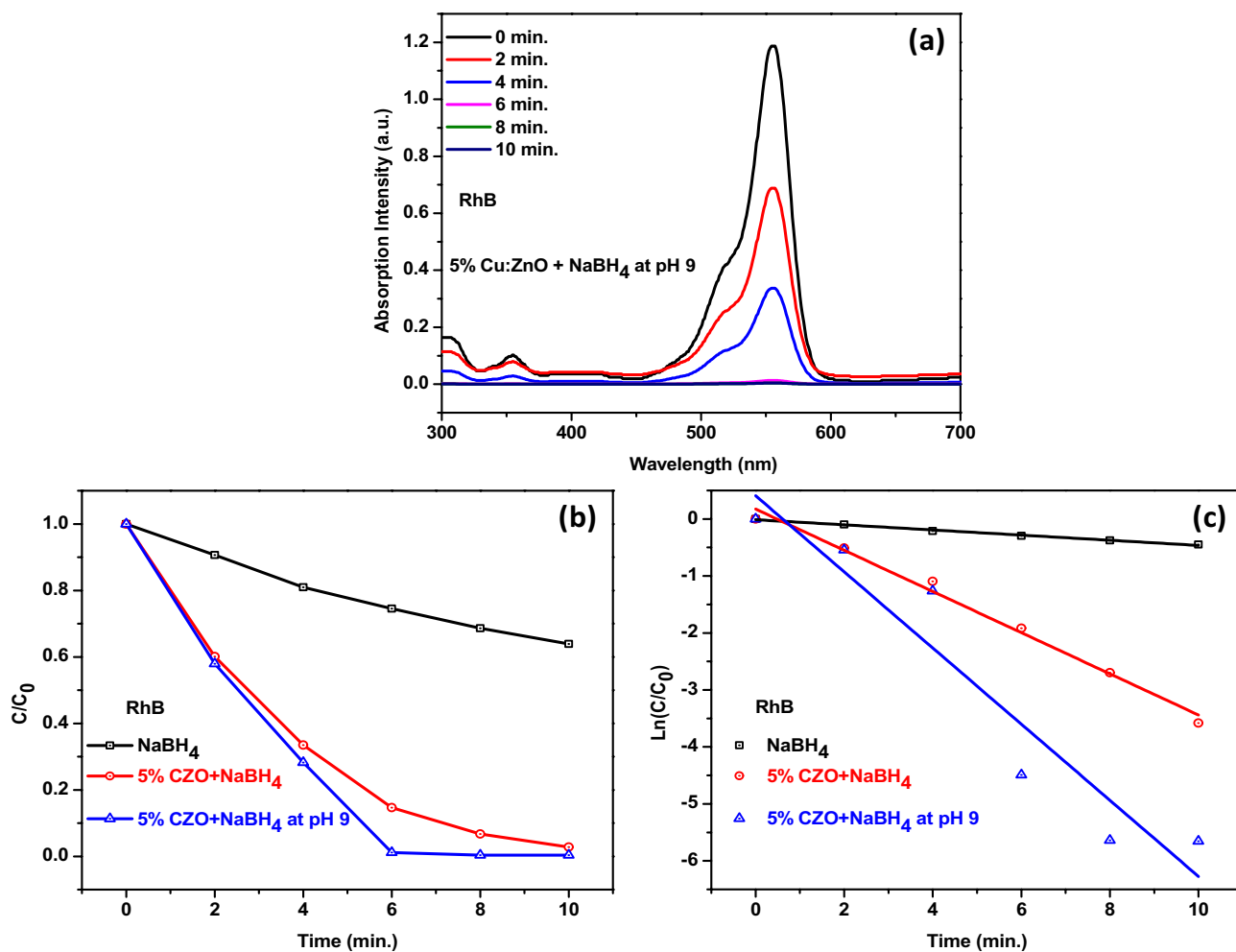


Fig. 9 **a** Time-dependent UV-absorption spectrum of RhB dye with (5 wt% Cu: ZnO) at pH 9 **b** Comparative C/C_0 versus reaction time and $\ln(C/C_0)$ versus reaction time of NaBH_4 , $\text{NaBH}_4 + 5 \text{ wt\% Cu: ZnO}$ and $\text{NaBH}_4 + 5 \text{ wt\% Cu: ZnO}$ at pH 9

Table 3 comparative catalytic measurements of RhB dye with respective catalyst

Materials	Dye used	Photocatalytic activity			
		R^2 value	Rate constant (k) ($\times 10^{-3} \text{ s}^{-1}$)	Reaction time (min)	Degradation percentage (%)
NaBH ₄	RhB	0.99222	45.12	10	36
ZnO + NaBH ₄	RhB	0.99754	88.15	10	58
1% Cu:ZnO + NaBH ₄	RhB	0.99901	116.42	10	69
3% Cu:ZnO + NaBH ₄	RhB	0.99178	177.84	10	82
5% Cu:ZnO + NaBH ₄	RhB	0.98784	361.36	10	97
5% Cu:ZnO + NaBH ₄ at pH 9	RhB	0.89097	668.26	6	99

Table 4 Comparative catalytic measurements of previously reported work with present work

S. no.	Materials	Dye	Reaction time (min)	Degradation percentage (%)	References
1	Ag/ZnO + NaBH ₄	MB	2	99	[35]
		CR	6	99	
		MO	4	99	
2	Ag + NaBH ₄	MB	13	98	[36]
3	CuO + NaBH ₄	CR	14	99	[37]
4	MgO/ZnO + NaBH ₄	MO	14	97	[38]
5	Ag/ZnO + NaBH ₄	MO	12	86	[39]
6	ZnS + NaBH ₄	MB	20	94	[40]
7	Cu:ZnO + NaBH ₄	RhB	10	97	Present work
8	Cu:ZnO + NaBH ₄ at pH 9	RhB	6	99	Present work

MB methylene blue, CR congo red, MO methyl orange, RhB rhodamine B

percentages for all the synthesized nanoparticles are comparatively listed in Table 3.

Conclusion

In overview, pure and Cu doped (1, 3, and 5 wt%) ZnO samples were progressively processed by precipitation process at ambient temperature. It is verified from XRD data that the whole material is of fine crystalline nature with a hexagonal structure of wurtzite. The lattice constants "a" and "c" suggest that with growing Cu density, Cu⁺, Cu²⁺ ions replace at the Zn location. The shift in unit cell volume may be attributable to the voids or defects creation mostly during diffusion process of Cu⁺, Cu²⁺, ions in the transition phase. The absorption spectral data suggest that, attributed to the impact of pressure, the value of the band gap energy varies. FTIR spectra assess the chemical groups of prepared samples from its transmittance IR peaks. The synthesized pure and Cu doped ZnO nanoparticles showed remarkable antibacterial activities against Escherichia coli and staphylococcus aureus. SEM image demonstrated the shape and

size of as-prepared samples. It is in good accordance at 2 μm magnification with XRD results. The catalytic activity of the prepared samples was analyzed with RhB textile dye and 99% of efficiency was achieved for 5 wt% Cu doped ZnO nanoparticles within 6 min at pH 9. Such that the synthesized Cu doped ZnO NPs is a potential remedy for catalytic degradation of textile dye as well as in the field of antibacterial activity (Table 4).

Declaration

Conflict of interest All the authors do not have any potential conflicts of interest.

References

1. A.B. Djuricic, A.M.C. Ng, X.Y. Chen, ZnO nanostructures for optoelectronics: material properties and device applications. *Prog. Quantum Electron.* **34**, 191–259 (2010)
2. C. Hanley, J. Layne, A. Punnoose, K.M. Reddy, I. Coombs, A. Coombs, K. Feris, D. Wingett, Preferential killing of cancer cells and activated human T cells using ZnO nanoparticles. *Nanotechnology* **19**, 10 (2008)

3. H.M. Xiong, Photoluminescent ZnO nanoparticles modified by polymers. *J. Mater. Chem.* **20**, 4251–4262 (2010)
4. H. Wang, D. Wingett, M.H. Engelhard, K. Feris, K.M. Reddy, P. Turner, J. Layne, C. Hanley, J. Bell, D. Tenne, C. Wang, A. Punnoose, Fluorescent dye encapsulated ZnO particles with cell-specific toxicity for potential use in biomedical applications. *J. Mater. Sci. Mater. Med.* **20**, 11–22 (2009)
5. Y.L. Liu, K.L. Ai, Q.H. Yuan, L.H. Lu, Fluorescence-enhanced gadolinium-doped zinc oxide quantum dots for magnetic resonance and fluorescence imaging. *Biomaterials* **32**, 1185–1192 (2011)
6. Y. Khan, S.K. Durrani, M. Mehmood, J. Ahmad, M.R. Khan, S. Firdous, Low temperature synthesis of fluorescent ZnO nanoparticles. *Appl. Surf. Sci.* **257**, 1756–1761 (2010)
7. H. Rotella, Y. Mazel, S. Brochen, A. Valla, A. Pautrat, C. Licitra, N. Rochat, C. Sabbione, G. Rodriguez, E. Nolot, Role of vacancy defects in Al doped ZnO thin films for optoelectronic devices. *J. Phys. D Appl. Phys.* **50**, 7 (2017)
8. F.B. Gu, D. You, Z.H. Wang, D.M. Han, G.S. Guo, Improvement of gas-sensing property by defect engineering in microwave-assisted synthesized 3D ZnO nanostructures. *Sens. Actuators B* **204**, 342–350 (2014)
9. R.S. Ganesh, E. Durgadevi, M. Navaneethan, V.L. Patil, S. Ponnusamy, C. Muthamizhchelvan, Y. Hayakawa, Tuning the selectivity of NH₃ gas sensing response using Cu-doped ZnO nanostructures. *Sens. Actuators A* **269**, 331–341 (2018)
10. L. Chow, O. Lupan, G. Chai, H. Khallaf, L.K. Ono, B.R. Cuenya, A. Schulte, Synthesis and characterization of Cu-doped ZnO one-dimensional structures for miniaturized sensor applications with faster response. *Sens. Actuators A* **189**, 399–408 (2013)
11. S. Thota, T. Dutta, J. Kumar, On the sol–gel synthesis and thermal, structural, and magnetic studies of transition metal (Ni Co, Mn) containing ZnO powders. *J. Phys. Condens. Matter* **18**(8), 2473 (2006)
12. S. Singhal, J. Kaur, T. Namgyal, R. Sharma, Cu-doped ZnO nanoparticles: synthesis, structural and electrical properties. *Phys. B* **407**(8), 1223–1226 (2012)
13. P.N. Kumar, M. Boovarasan, R.K. Singh, S. Kannan, Synthesis, structural analysis and fabrication of coatings of the Cu²⁺ and Sr²⁺ co-substitutions in β-Ca₃(PO₄)₂. *RSC Adv.* **3**(44), 22469–22479 (2013)
14. E.J. Elzinga, R.J. Reeder, X-ray absorption spectroscopy study of Cu²⁺ and Zn²⁺ adsorption complexes at the calcite surface: implications for site-specific metal incorporation preferences during calcite crystal growth. *Geochim. Cosmochim. Acta* **66**(22), 3943–3954 (2002)
15. K. Omri, A. Bettaibi, K. Khirouni, L. El Mir, The optoelectronic properties and role of Cu concentration on the structural and electrical properties of Cu doped ZnO nanoparticles. *Phys. B* **537**, 167–175 (2018)
16. R. Elilarassi, G. Chandrasekaran, Structural, optical and magnetic characterization of Cu-doped ZnO nanoparticles synthesized using solid state reaction method. *J. Mater. Sci. Mater. Electron.* **21**(11), 1168–1173 (2010)
17. M. Fu, Y. Li, P. Lu, J. Liu, F. Dong, Sol–gel preparation and enhanced photocatalytic performance of Cu-doped ZnO nanoparticles. *Appl. Surf. Sci.* **258**(4), 1587–1591 (2011)
18. M. Mittal, M. Sharma, O.P. Pandey, UV–visible light induced photocatalytic studies of Cu doped ZnO nanoparticles prepared by co-precipitation method. *Sol. Energy* **110**, 386–397 (2014)
19. K.G. Kanade, B.B. Kale, J.O. Baeg, S.M. Lee, C.W. Lee, S.J. Moon, H. Chang, Self-assembled aligned Cu doped ZnO nanoparticles for photocatalytic hydrogen production under visible light irradiation. *Mater. Chem. Phys.* **102**(1), 98–104 (2007)
20. L.B. Saad, L. Soltane, F. Sediri, Pure and Cu-doped ZnO nanoparticles: hydrothermal synthesis, structural, and optical properties. *Russ. J. Phys. Chem. A* **93**(13), 2782–2788 (2019)
21. M. Fang, C.M. Tang, Z.W. Liu, Microwave-assisted hydrothermal synthesis of Cu-doped ZnO single crystal nanoparticles with modified photoluminescence and confirmed ferromagnetism. *J. Electron. Mater.* **47**(2), 1390–1396 (2018)
22. A. Goktas, F. Aslan, A. Tumbul, Nanostructured Cu-doped ZnS polycrystalline thin films produced by a wet chemical route: the influences of Cu doping and film thickness on the structural, optical and electrical properties. *J. Sol–Gel. Sci. Technol.* **75**(1), 45–53 (2015)
23. U.P.S. Gahlaut, V. Kumar, R.K. Pandey, Y.C. Goswami, Highly luminescent ultra small Cu doped ZnO nanostructures grown by ultrasonicated sol–gel route. *Optik* **127**(10), 4292–4295 (2016)
24. L.C.K. Liau, J.S. Huang, Energy-level variations of Cu-doped ZnO fabricated through sol-gel processing. *J. Alloys Compd.* **702**, 153–160 (2017)
25. M.F. Manamela, Structural, optical and sensing properties of cobalt and indium doped zinc oxide prepared mechano-chemically. Doctoral dissertation (2018)
26. U. Manzoor, S. Siddique, R. Ahmed, Z. Noreen, H. Bokhari, I. Ahmad, Antibacterial, structural and optical characterization of mechano-chemically prepared ZnO nanoparticles. *PLoS ONE* **11**(5), e0154704 (2016)
27. S. Roguai, A. Djelloul, A structural and optical properties of Cu-doped ZnO films prepared by spray pyrolysis. *Appl. Phys. A* **126**(2), 1–8 (2020)
28. P.S. Shewale, V.B. Patil, S.W. Shin, J.H. Kim, M.D. Uplane, H₂S gas sensing properties of nanocrystalline Cu-doped ZnO thin films prepared by advanced spray pyrolysis. *Sens. Actuators B Chem.* **186**, 226–234 (2013)
29. A. Rahmati, A.B. Sirgani, M. Molaee, M. Karimipour, Cu-doped ZnO nanoparticles synthesized by simple co-precipitation route. *Eur. Phys. J. Plus* **129**(11), 1–7 (2014)
30. S. Muthukumar, R. Gopalakrishnan, Structural, FTIR and photoluminescence studies of Cu doped ZnO nanopowders by co-precipitation method. *Opt. Mater.* **34**(11), 1946–1953 (2012)
31. A. Pramothkumar, N. Senthilkumar, K.M.G. Malar, M. Meena, I.V. Potheher, A comparative analysis on the dye degradation efficiency of pure Co, Ni and Mn-doped CuO nanoparticles. *J. Mater. Sci. Mater. Electron.* **30**(20), 19043–19059 (2019)
32. M. Mazhdi, M.J. Tafreshi, The effects of gadolinium doping on the structural, morphological, optical, and photoluminescence properties of zinc oxide nanoparticles prepared by co-precipitation method. *Appl. Phys. A* **124**(12), 1–8 (2018)
33. C. Pholnak, C. Sirisathitkul, S. Suwanboon, D.J. Harding, Effects of precursor concentration and reaction time on sonochemically synthesized ZnO nanoparticles. *Mater. Res.* **17**, 405–411 (2014)
34. Z.M. Gibbs, A. LaLonde, G.J. Snyder, Optical band gap and the Burstein–Moss effect in iodine doped PbTe using diffuse reflectance infrared Fourier transform spectroscopy. *New J. Phys.* **15**(7), 075020 (2013)
35. A. Yeganeh-Faal, M. Bordbar, N. Negahdar, M. Nasrollahzadeh, Green synthesis of the Ag/ZnO nanocomposite using *Valeriana officinalis* L. root extract: application as a reusable catalyst for the reduction of organic dyes in a very short time. *IET Nanobiotechnol.* **11**(6), 669–676 (2017)
36. N.N. Bonnia, M.S. Kamaruddin, M.H. Nawawi, S. Ratim, H.N. Azlina, E.S. Ali, Green biosynthesis of silver nanoparticles using ‘Polygonum Hydropiper’ and study its catalytic degradation of methylene blue. *Procedia Chem.* **19**, 594–602 (2016)
37. M. Narasaiah, B.K. Mandal, N.C. Sarada, Biosynthesis of copper oxide nanoparticles from *Drypetes sepiaria* leaf extract and their catalytic activity to dye degradation, in *IOP Conference Series:*

- Materials Science and Engineering*, vol. 263, no. 2 (IOP Publishing, 2017), p. 022012
38. J. Maruthai, A. Muthukumarasamy, B. Baskaran, Optical, biological and catalytic properties of ZnO/MgO nanocomposites derived via *Musa paradisiaca* bract extract. *Ceram. Int.* **44**(11), 13152–13160 (2018)
 39. K.U.R.U. Mehmet, S. Pekdemir, Polydopamine mediated growth of Ag nanostructures on ZnO thin films for catalytic degradation of organic dyes. *Gazi Univ. J. Sci.* **33**(4), 857–870 (2020)
 40. A. Rafiq, M. Imran, M. Ikram, M. Naz, M. Aqeel, H. Majeed, S.G. Hussain, S. Ali, Photocatalytic and catalytic degradation of organic dye by uncapped and capped ZnS quantum dots. *Mater. Res. Express* **6**(5), 055801 (2019)